ISSN 1674-1056
http://cpb.iphy.ac.cn
http://iopscience.iop.org/cpb
中国物理 B
Chinese Physics
中国物理
Chinese Physics B

Time-dependent crosstalk effects for image sensors with different isolation structures

Lei Shen(沈磊), Li-Qiao Liu(刘力桥), Hao Hao(郝好), Gang Du(杜刚), Xiao-Yan Liu(刘晓彦)

Citation: Chin. Phys. B . 2018, 27(8): 088503. **doi:** 10.1088/1674-1056/27/8/088503

Journal homepage: http://cpb.iphy.ac.cn; http://iopscience.iop.org/cpb

What follows is a list of articles you may be interested in

Organic photovoltaic cells with copper (Ⅱ) tetra-methyl substituted phthalocyanine

Xu Zong-Xiang, Roy V. A. L.

Chin. Phys. B . 2013, 22(12): 128505. **doi:** 10.1088/1674-1056/22/12/128505

Multifunctional silicon-based light emitting device in standard complementary metal–oxide–semiconductor technology

Wang Wei, Huang Bei-Ju, Dong Zan, Chen Hong-Da

Chin. Phys. B . 2011, 20(1): 018503. **doi:** 10.1088/1674-1056/20/1/018503

Time-dependent crosstalk effects for image sensors with different isolation structures*

Lei Shen(沈磊), Li-Qiao Liu(刘力桥), Hao Hao(郝好), Gang Du(杜刚), and Xiao-Yan Liu(刘晓彦)†

Institute of Microelectronics, Peking University, Beijing 100871, *China*

(Received 22 February 2018; revised manuscript received 16 April 2018; published online 10 July 2018)

Photo-generated carriers may diffuse into the adjacent cells to form the electrical crosstalk, which is especially noticeable after the pixel cell size has been scaled down. The electrical crosstalk strongly depends on the structure and electrical properties of the photosensitive areas. In this work, time-dependent crosstalk effects considering different isolation structures are investigated. According to the different depths of photo-diode (PD) and isolation structure, the transport of photo-generated carriers is analyzed with different regions in the pixel cell. The evaluation of crosstalk is influenced by exposure time. Crosstalk can be suppressed by reducing the exposure time. However, the sensitivity and dynamic range of the image sensor need to be considered as well.

Keywords: image sensor, crosstalk, pixel isolation

PACS: 85.60.–q **DOI:** 10.1088/1674-1056/27/8/088503

1. Introduction

Image sensors are widely used in military, medical, automotive, and mobile devices.[1] With the continuous increase of application areas, the requirement for imaging quality becomes higher and the size of a pixel cell keeps on scaling down.[2–6] Optical or electrical crosstalk may occur between adjacent pixel cells.[7,8] Photons enter into the adjacent pixel cells before they are absorbed by the photosensitive areas, thus producing optical crosstalk. The optical crosstalk can be suppressed by optimizing the interconnected structures above the devices or using the backside illumination structures.[9–11] The photons absorbed by the photosensitive areas and converted into photo-generated carriers may diffuse into the adjacent cells to form the electrical crosstalk. The optimization of photosensitive areas and the introduction of isolation structures could restrain the electrical crosstalk.[7,8,12,13] The crosstalk would reduce the quantum efficiency indirectly and affect the imaging quality. This crosstalk is especially noticeable after the pixel cell size has been scaled down to approximately one micrometer.

The electrical crosstalk strongly depends on the structure and electrical properties of the photosensitive area. Deep trench isolation (DTI)[7,8,13,14] and heavy doping isolation[15,16] are employed to resist the electrical crosstalk currently. In smaller pixel cells, the width of the isolation structure also requires a corresponding reduction, which becomes a greater challenge to the process. Therefore, the influence of crosstalk needs to be systematically studied for designing and optimizing the pixel structures with different isolation structures. Different methods have been employed to study the crosstalk between pixel cells. Some researchers directly measured the crosstalk experimentally.[7,8] Due to the small number of experimental samples, the influences of pixel size and isolation structures on crosstalk may not be systematically studied. In addition, the exposure time is usually fixed experimentally. Hence the time-dependent crosstalk effect cannot be studied. On the other hand, some researches have been conducted using models or simulations.[17–20] However, most of the models did not consider isolation structures. For small pixel cells, the large aspect ratio of the photosensitive area makes the isolation structure indispensable, and the crosstalk models should consider the influence of the isolation structure. Moreover, most of the crosstalk models and simulations are the steady-state solutions of drift-diffusion equations. However, in the actual image sensor, the electrical crosstalk is the time-dependent diffusion process of photo-generated carriers. Especially for the case of low light intensity, the steady state cannot be reached within the exposure time. The influence of exposure time should be considered in the study of crosstalk.

In this work, time-dependent crosstalk effects considering different isolation structures are proposed. According to the different depths of PD and isolation structures, the transport of photo-generated carrier is modeled with different regions in the pixel cell. By using the technology computer aided design (TCAD) tool, the time-dependent crosstalk effects are evaluated for the carriers' transport with incident light of different wavelengths, and the isolation structures with different DTI depths. The results can help to design and optimize the image sensor especially for scaling down the pixel size.

*Project supported by the National Key Research and Development Program of China (Grant No. NKRDP 2016YFA0202101).

†Corresponding author. E-mail: xyliu@ime.pku.edu.cn

© 2018 Chinese Physical Society and IOP Publishing Ltd

2. Image sensor structure and crosstalk

The main area of a pixel cell is the photosensitive area. Therefore, a photosensitive structure with adjacent cells is analyzed as shown in Fig. 1. The main parameters are listed in Table 1. Each cell has an independent top contact, and the public bottom contact is used. The isolation is located between adjacent cells, and a 30-nm-thick $P+$ passivation layer is used around the DTI region in order to reduce the interface effect.

According to the different depths of pinning layer (PIN), PD and isolation structure, the pixel cell can be partitioned into several regions as shown in Figs. 1(a) and 1(b). The photo-generated carriers drift and diffuse between various regions under the influence of electric field and concentration gradient. Photo-generated carriers in each region are affected by different conditions, and their transports are different.

Table 1. Parameters used in this work.

Parameter	Value
Pixel width	1.5 μm
Pixel depth	4 μm
Photo-diode width	1 μm
Photo-diode depth	0.8 μm
DTI width	100 nm
DTI depth	0.5–3 μm
Photo-diode doping	5×10^{16} cm^{-3}
Well doping	1×10^{15} cm^{-3}
P+ layer doping	1×10^{18} cm^{-3}

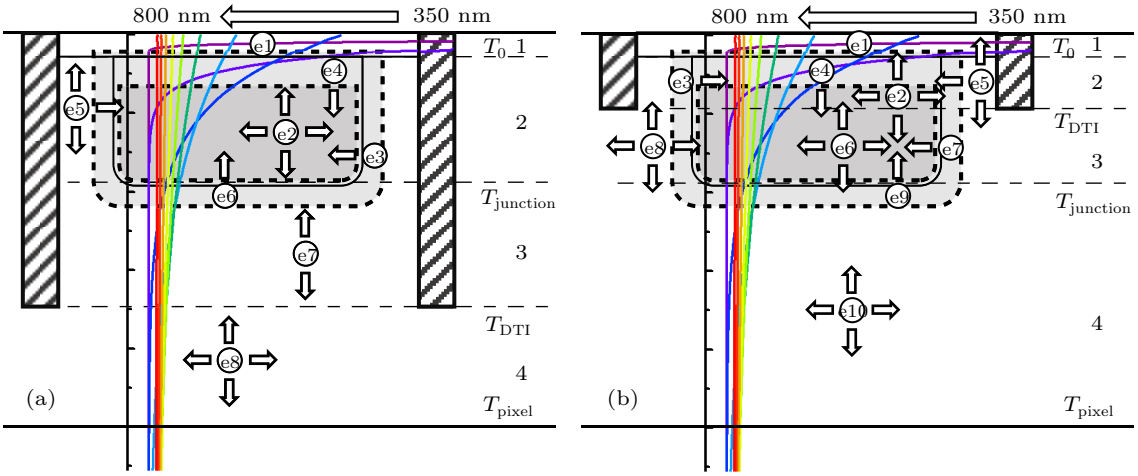


Fig. 1. (color online) Schematic diagram of partitioned crosstalk region, showing (a) depth of DTI greater than the depth of PD structure, (b) depth of DTI less than thte depth of PD structure.

Figure 1(a) shows the case where the depth of DTI is greater than the depth of PD structure. According to the different depths of pinning layer, PD and isolation structure, the pixel cell is divided into four depth ranges, and photo-generated electrons can appear in eight regions.

Electrons in e1: most recombined in pinning layer.

Electrons in e2: diffusion to the depletion zone under the influence of concentration gradient.

Electrons in e3, e4, and e6: accumulated in the depletion zone edge under the influence of electric field.

Electrons in e5 and e7: diffusion upward, downward, and to the depletion zone under the influence of concentration gradient.

Electrons in e8: diffusion around under the influence of concentration gradient.

The diffusion of electrons in e8 to adjacent pixel cells results in crosstalk.

Figure 1(b) shows the case where the depth of DTI is less than the depth of PD structure. According to the different depths of PD, pinning layer and isolation structure, the pixel cell is divided into four depth ranges, and photo-generated electrons can appear in ten regions.

Electrons in e1: most recombined in the pinning layer.

Electrons in e2 and e6: diffusion to the depletion zone under the influence of concentration gradient.

Electrons in e3, e4, e7, and e9: accumulated in the depletion zone edge under the influence of electric field.

Electrons in e5: diffusion upward, downward, and to the depletion zone under the influence of concentration gradient.

Electrons in e8 and e10: diffusion around and to the depletion zone under the influence of concentration gradient.

The diffusion of electrons in e8 and e10 to adjacent pixel cells results in crosstalk.

Combining photon absorption rates and drift-diffusion equation (Eq. (1)) in different regions, the time-dependent crosstalks can be obtained with different boundary conditions.

$$-D_p\nabla^2 p(x,y)+\frac{p(x,y)}{\tau_p}=\phi_0\cdot\alpha\cdot \mathrm{e}^{-\alpha y}\cdot\delta(x). \qquad (1)$$

The Sentaurus TCAD tool[21] is used to simulate the electrical and optical characteristics. The input optical signals

are introduced by the raytracing method, and the photons absorbed by the photosensitive areas are converted into photo-generated carriers. The number of electrons increasing after illumination in each pixel cell is integrated to obtain the number of photo-carriers accumulated in the pixel cell. The ratio of the average number of photo-carriers of adjacent pixel cells to the number of photo-carriers of the illuminated cells is defined as the crosstalk value. The light intensities at different wavelengths are finely adjusted such that the incident photon numbers with different wavelengths are equal. The physical models include the drift-diffusion model, the SRH combination model, and the high field saturation model. Due to the fact that the study focuses on electrical crosstalk of photo-generated carriers, neither the diffraction nor the crosstalk of light is considered in this work.

3. Results and discussion

3.1. Influence of incident light wavelength

As shown in Fig. 1, the color curves in the figure show the relationship between the number of absorbed photons and the depth of photosensitive region with incident light of different wavelengths. When the wavelength is short, the absorption coefficient in the silicon is large, and photons are mainly absorbed in the shallower region. As the wavelength increases, the absorption coefficient decreases, and the absorb region extends. Then the photon absorption in the shallower region is reduced and the photon absorption in the deeper region is increased. The accumulated electron density and electron current density profiles for 400-nm, 500-nm, and 750-nm incident light at three exposure times (initial, accumulated, and stabilized) are shown in Figs. 2 and 3, respectively. The carrier diffusion process causing crosstalk described above can be seen in the figures. The typical positions of the photo-generated carriers and the corresponding movement paths are marked in the figures of 40 μs.

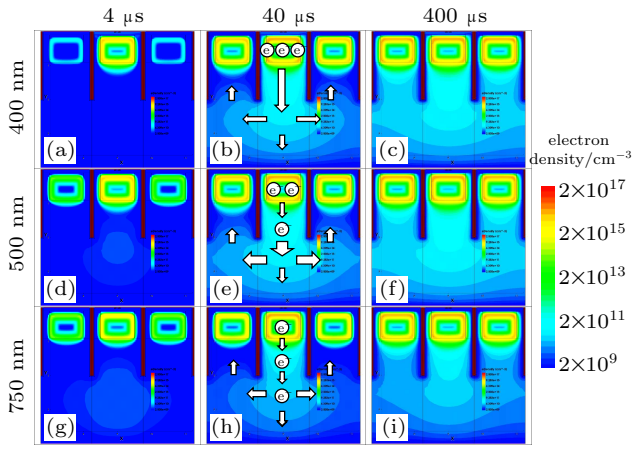


Fig. 2. (color online) Accumulated electron density profiles for 400-nm, 500-nm, and 750-nm incident light at three exposure times.

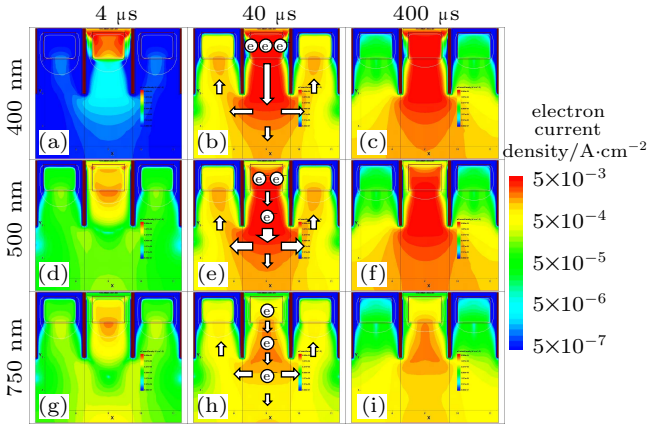


Fig. 3. (color online) Electron current density profiles for 400-nm, 500-nm, and 750-nm incident light at three exposure times.

At the beginning of exposure, the longer the incident wavelength of light, the more photo-generated carriers are absorbed in the substrate as shown in Figs. 2(a), 2(d), and 2(g). These photo-generated carriers diffuse under the influence of the concentration gradient. The upward diffusion will accumulate in the PD area, and the diffusion toward the adjacent pixel cells will produce crosstalk. As can be seen in Fig. 3(a), the 400-nm-wavelength photons are mainly absorbed at the surface, and the absorption depth is about 0.1 μm. In addition to the recombination in the pinning layer, the remaining electrons diffuse down to the depletion region, and the number of electrons that diffuse to adjacent cells is small. The absorption of 500-nm-wavelength photons is deeper whose absorption depth is about 0.5 μm, and in addition to the accumulation of carriers in the PD area, the diffusion towards the adjacent cells produces crosstalk. The 750-nm wavelength photons are absorbed in the entire depth direction whose absorption depth is about 10 μm, the number of carriers accumulated in the PD area is smallest, and the number of carriers diffused to the adjacent cells is largest. Therefore, the crosstalk is largest at this time. The number of accumulated carriers and the crosstalk versus the wavelength of incident light, for different exposure times, are plotted in Figs. 4 and 5, respectively. At the beginning of exposure, the number of accumulated carriers with shorter wavelength in the illumination cell is larger, while that with longer wavelength is smaller, as described above. The number of accumulated carriers with 450-nm wavelength is four times larger than that with 800-nm wavelength. For the case of wavelength less than 400 nm, photons are mainly absorbed in the pinning layer and the photo-generated carriers are recombined. Therefore, the accumulated carriers decrease. The number of accumulated carriers increases in the adjacent cells as the wavelength increases. Accordingly, the crosstalk increases as the wavelength increases, as indicated with the black curve in Fig. 5. The crosstalk is less than 10% at the beginning of exposure, and the maximum value is only 6.2% whose wavelength is 800 nm.

At the time of accumulation as shown in Figs. 3(b), 3(e), and 3(h), the diffusion to the adjacent cells with smaller wavelength becomes larger. The accumulated carriers of the illumination cell are stabilized, while the carriers of the adjacent cells increase rapidly as shown in Fig. 4. However, for the case that wavelength is larger, part of the photons cannot be absorbed through the photosensitive area, and the absorbed photo-carriers are distributed over the entire depth range. The accumulation in PD area does not yet reach a steady state, and the diffusion to adjacent cells is relatively small. The accumulated carriers in adjacent cells with 800-nm wavelength is only one-fifth of the carriers with 500-nm wavelength as shown in Fig. 4. The crosstalk with different wavelengths at 40 μs is plotted in Fig. 5. Except for larger wavelengths, the crosstalk is about 50%. The peak value of crosstalk occurs around 500-nm wavelength at the time of accumulation, and the human eye has the highest sensitivity in this wavelength range, so image sensors should be carefully optimized to reduce crosstalk. The accumulation in the illumination cell and adjacent cells are not stabilized with a larger wavelength. Hence both numbers of accumulated carriers increase at the same time and the change of crosstalk is relatively small, which is just greater than 10%.

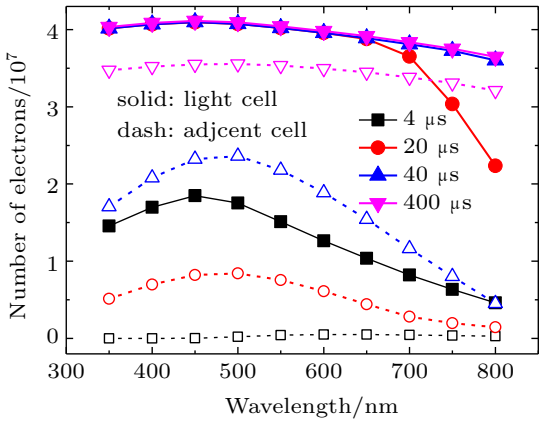


Fig. 4. (color online) Variations of the number of accumulated electrons with wavelength at different exposure times.

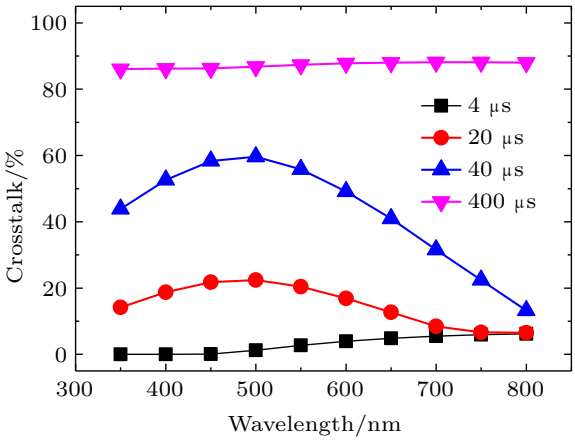


Fig. 5. (color online) Variations of crosstalk with wavelength at different exposure times.

When the steady state is reached, the carriers in the illumination cell diffuse mainly to the substrate. In the case of the same number of incident photons, due to the fact that the partial photons are not absorbed by the photosensitive region with larger wavelength, the number of accumulated electric carriers and the electron current density are smaller under steady state as shown in Figs. 2(c), 2(f), and 2(i) and Figs. 3(c), 3(f), and 3(i). The crosstalk is almost 87% with different wavelengths as shown in Fig. 5. Because more photons are absorbed in the area below the depth of the DTI, the crosstalk with 800-nm wavelength after stabilization is 2% higher than that with 350-nm wavelength.

When considering the time-dependent crosstalk effect, the trends of crosstalk versus wavelength are different for different exposure times. The human eyes are more sensitive to the green wavelength range, which is not the most serious case of crosstalk at the beginning of exposure and stable state. However, in the exposure process, the crosstalk is the most serious. Evaluation of crosstalk using only a stable condition would not give the actual trend for different exposure times.

3.2. Influence of DTI depth

As described in Section 2, the depth of DTI structure can affect the transport of photo-generated carriers. DTI structures at different depths have different effects on the time-dependent crosstalk properties of photo-generated carriers. The densities of accumulated electrons with DTI depths ranging from 0.5 μm to 3 μm are plotted in Fig. 6. The wavelength of incident light is 550 nm. The electron density profiles with 2-μm DTI depth are shown in Figs. 2(d)–2(f).

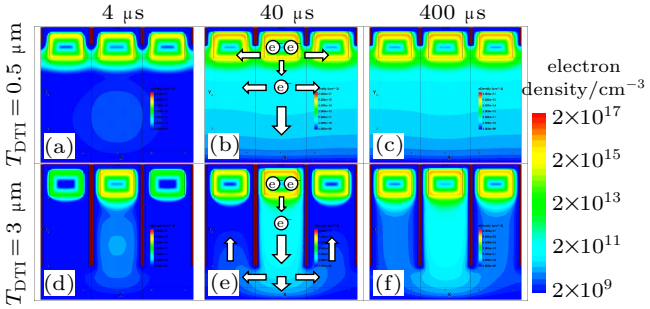


Fig. 6. (color online) Accumulated electron density profiles with DTI thickness values of 0.5 μm and 3 μm at three exposure times.

When the DTI depth is less than the PD depth as the case in Fig. 1(b), the electrons in regions e8 and e10 may diffuse to adjacent cells. Hence the crosstalk is serious, even if in the early exposure, the crosstalk is higher than 99% as plotted in Fig. 7.

When the DTI depth is greater than the PD depth as the case in Fig. 1(a), most photo-carriers need to undergo downward diffusion, lateral diffusion, and upward diffusion to form carriers' accumulation in adjacent cells as shown in Fig. 6(e).

At the beginning of the exposure, the accumulation of the illumination cells has not yet reached a steady state and the component of the downward diffusion is small. Hence the crosstalk is almost less than 5%. As the exposure time increases, crosstalk begins to increase. The smaller the DTI depth is, the faster the crosstalk increases due to the fact that the path of diffusion is shorter. After stabilization, the values of crosstalk with different DTI depths are all larger than 75%, and the deeper the DTI is, the smaller the crosstalk is.

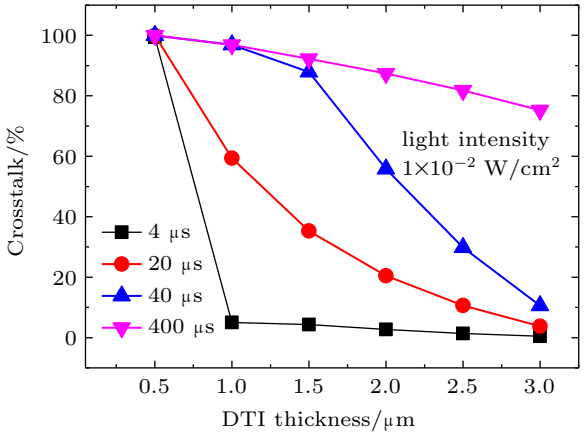


Fig. 7. (color online) Relations between crosstalk and DTI thickness at different exposure times.

As the image sensor will use a suitable exposure time for better sensitivity and appropriate dynamic range in actual use, the stabilization of photo-carriers accumulation will not be reached for a common incident light intensity. Therefore, the crosstalk evaluation of the pixel cell and the isolation structure is a time-dependent photo-carriers' diffusion problem. On the other hand, in some special applications, shortening the exposure time can effectively reduce the crosstalk caused by photo-carriers' diffusion.

4. Conclusions

In this work, a time-dependent crosstalk effect has been investigated. According to the different depths of PD and isolation structure, the pixel cell is partitioned into several regions. Photo-generated carriers have different motions in different regions. Only the carriers that have spread to adjacent cells can cause the crosstalk. The evaluation of crosstalk is influenced by the exposure time. The crosstalk can be reduced by reducing the exposure time but will lose the sensitivity and dynamic range. The results can help to design and optimize the image sensor especially for scaling down the pixel size.

References

[1] Willner A E, Byer R L, Chang-Hasnain C J, Forrest S R, Kressel H, Kogelnik H, Kogelnik H, Tearney G J, Townes C H and Zervas M N 2012 *Proc. IEEE* **100** 1604

[2] Lei C, Ozeki Y and Goda K 2017 *Proceedings of the International Image Sensor Workshop*, May 30–June 2, 2017, Hiroshima, Japan, I2

[3] Tanioka K 2017 *Proceedings of the International Image Sensor Workshop*, May 30–June 2, 2017, Hiroshima, Japan, I3

[4] Miyazaki S 2017 *Proceedings of the International Image Sensor Workshop*, May 30–June 2, 2017, Hiroshima, Japan, I4

[5] Wang F, Li Y D, Guo Q, Wang B, Zhang X Y, Wen L and He C F 2016 *Acta Phys. Sin.* **65** 024212 (in Chinese)

[6] Chen C, Bing Z, Wu L S, Li N and Wang J F 2014 *Chin. Phys. B* **23** 124215

[7] Tournier A, Leverd F, Favennec L, Perrot C, Pinzelli L, Gatefait M, Cherault N, JeanJean D, Carrere J P, Hirigoyen F, Grant L and Roy F 2011 *Proceedings of the International Image Sensor Workshop*, June 8–June 11, 2011, Hokkaido, Japan, R5

[8] Kitamura Y, Aikawa H, Kakehi K, Yousyou T, Eda K, Minami T, Uya S, Takegawa Y, Yamashita H, Kohyama Y and Asami T 2012 *Digest of IEEE International Electron Devices Meeting*, December 10–12, 2012, San Francisco, USA, 24.2.1

[9] Sukegawa S, Umebayashi T, Nakajima T, Kawanobe H, Koseki K, Hirota I, Haruta T, Kasai M, Fukumoto K, Wakano T, Inoue K, Takahashi H, Nagano T, Nitta Y, Hirayama T and Fukushima N 2013 *Digest of IEEE International Solid-State Circuits Conference*, February 17–21, 2013, San Francisco, USA, 484

[10] Choi S, Lim S H, Lim M, Bae H J, Choo K J, Park J H, Lee K S, Kim S S, Moon J, Son K, Shim E S, Cho H, Kim Y, Ham S H, Ahn J C, Moon C R and Lee D 2015 *Proceedings of the International Image Sensor Workshop*, June 8–11, 2015, Vaals, Netherlands, I4

[11] Kato Y, Sano T, Moriyama Y, Maeda S, Yamazaki T, Nose A, Shina K, Yasu Y, Tempel W, Ercan A and Ebiko Y 2017 *Proceedings of Symposium of VLSI Circuits*, June 5–8, 2017, Kyoto, Japan, C288

[12] Shinohara T, Watanabe K, Arakawa S, Kawashima H, Kawashima A, Abe T, Yanagita T, Ohta K, Inada Y, Onizuka M, Nakayama H, Tateshita Y, Morikawa T, Ohno K, Sugimoto D, Kadomura S and Hirayama T 2013 *Digest IEEE International Electron Devices Meeting*, December 9–11, 2013, San Francisco, USA, 27.4.1

[13] Park B J, Jung J, Moon C R , Hwang S H, Lee Y W, Kim D W, Paik K H, Yoo J R, Lee D H and Kim K 2007 *Jpn. J. Appl. Phys.* **46** 2454

[14] Choi S, Lee K, Yun J, Choi S, Lee S, Park J, Shim E S, Pyo J, Kim B, Jung M, Lee Y, Son K, Jung S, Wang T S , Choi Y, Min D K , Im J, Moon C R , Lee D and Chang D 2017 *Proceedings of Symposium on VLSI Technology*, June 5–8, 2017, Kyoto, Japan, T104

[15] Furumiya M, Ohkubo H, Muramatsu Y, Kurosawa S, Okamoto F, Fujimoto Y and Nakashiba Y 2001 *IEEE Trans. Electron. Dev.* **48** 2221

[16] David Y and Efron U 2006 *Proceedings of IEEE 24th Convention of Electrical and Electronics Engineers in Israel*, November 15–17, 2006, Eilat, Israel, 67

[17] Shcherback I, Danov T and Yadid-Pecht O 2004 *IEEE Trans. Electron. Dev.* **51** 2033

[18] Djite I, Estribeau M, Magnan P, Roll, G, Petit S and Saint-Pe O 2012 *IEEE Trans. Electron. Dev.* **59** 729

[19] Blanco-Filgueira B, López P and Roldán J B 2013 *IEEE Trans. Electron. Dev.* **60** 3459

[20] Blanco-Filgueira B, Martínez P L, Aranda J B R and Hauer J 2015 *IEEE Trans. Electron. Dev.* **62** 580

[21] *Synopsys Sentaurus T C A D User's Manual*, H-2013.03, 2013